Optical conductivity of the icosahedral quasicrystal $Al_{75.5}Mn_{20.5}Si_4$ and its 1/1 crystalline approximant alpha -$Al_{72.5}Mn_{17.4}Si_{10.1}$

1993 J. Phys.: Condens. Matter 5 5975

(http://iopscience.iop.org/0953-8984/5/32/026)

J. Phys.: Condens. Matter 5 (1993) 5975–5990. Printed in the UK

Optical conductivity of the icosahedral quasicrystal $Al_{75.5}Mn_{20.5}Si_4$ and its 1/1 crystalline approximant α-$Al_{72.5}Mn_{17.4}Si_{10.1}$

X Wu†, C C Homes†, S E Burkov†, T Timusk†, F S Pierce‡, S J Poon‡, S L Cooper§ and M A Karlow§

† Department of Physics and Astronomy, McMaster University, Hamilton, Ontario, Canada L8S 4M1

‡ Department of Physics, University of Virginia, Charlottesville, Virginia 22901, USA

§ Department of Physics and Materials Research Laboratory, University of Illinois at Urbana-Champaign, Urbana IL 61801, USA

Received 2 March 1993, in final form 4 May 1993

Abstract. The reflectance of the metastable icosahedral quasicrystal $Al_{75.5}Mn_{20.5}Si_4$ and its 1/1 crystalline approximant α-$Al_{72.5}Mn_{17.4}Si_{10.1}$ has been measured from 50 cm^{-1} to 46 000 cm^{-1} at temperatures from $\approx$ 10 K to 295 K. The optical conductivity of the icosahedral sample is similar to that reported for the stable quasicrystal $Al_{63.5}Cu_{24.5}Fe_{12}$; starting out from a low DC value it rises linearly with frequency up to $\approx$ 1 eV reaching a maximum at $\approx$ 2.2 eV with a magnitude that is comparable with transition metals, above which it decreases slowly. The conductivity of the approximant phase is similar in shape, but the overall magnitude is lower. There is a broad structure at 200 cm^{-1} in the quasicrystal which is resolved into at least nine sharp phonon lines in the approximant. Band structure calculations of the crystalline approximant predict a pseudogap in the electronic density of states at the Fermi surface suggesting that the unusual optical properties of the icosahedral material may also be explained by band structure arguments.

1. Introduction

Since the first report of a metallic phase in AlMn alloys with an icosahedral (i) point group symmetry and no translational symmetry [1], many other alloys have been observed to exhibit icosahedral (as well as other non-crystallographic) symmetries [2–5] and a large body of experimental and theoretical work now exists on the effects of quasicrystalline order [6]. Some of the most frequently studied icosahedral systems are the Al-based ternary alloys containing transition metals such as the metastable AlMnSi system and the stable AlCu(Fe, Ru) systems [7,8]. Anomalous electronic properties have been observed [9] in these systems, including low densities of states (DOS) (as low as 10% of the free electron value in $Al_{65}Cu_{20}Ru_{15}$ [10]) and high resistivities (11 000 $\mu\Omega$ cm in $Al_{62.5}Cu_{25}Fe_{12.5}$ [11] and as high as 30 000 $\mu\Omega$ cm in $Al_{65}Cu_{20}Ru_{15}$ [10] at low temperature). The optical conductivity of $Al_{63.5}Cu_{24.5}Fe_{12}$ was found to exhibit an unusual linear frequency dependence and an absence of the usual Drude conductivity seen in metals [12]. By studying related phases such as the crystalline approximant phases, further insight can be gained concerning the electronic properties that are unique to a perfect quasicrystal.

Through structural studies [13], the 1/1 crystalline approximant α-AlMnSi has been determined to consist of 54-atom Mackay icosahedron clusters [14] which pack into a simple cubic structure with 138 atoms per unit cell. Structural studies have also provided convincing support to the proposal that the atomic decorations of the building blocks in the

0953-8984/93/325975+16$07.50

i-phases are related to the approximant phases [6]. Thus, it should be possible to learn about the effects of quasiperiodicity on electronic properties through comparison of an icosahedral phase with one of its approximant phases.

Band-structure calculations have been performed on crystalline approximants of quasicrystals for α-(AlMn) [15] as well as AlCuLi and AlFe [16]. In each case, the calculated density of states shows a pseudogap at the Fermi surface which satisfies a Hume–Rothery type relation. The recent measurement of the optical conductivity of the stable icosahedral quasicrystal $Al_{63.5}Cu_{24.5}Fe_{12}$ shows a depression below ≈ 1.4 eV and an almost total absence of free carriers [12], in agreement with the predictions of a pseudogap.

In this paper we examine the optical conductivity of the metastable icosahedral quasicrystal $Al_{75.5}Mn_{20.5}Si_4$, and the low-order 1/1 approximant phase α-$Al_{72.5}Mn_{17.4}Si_{10.1}$. Band-structure calculations have been performed for the approximant phase [15, 17] and predict a pseudogap in the DOS at the Fermi surface. Not only in the approximant phase is this predicted behaviour observed, but also in the icosahedral phase. The fact that the 1/1 approximant phase strongly resembles the *i*-phase suggests that band structure effects are responsible for the low DOS and the unusual optical properties of both systems.

2. Experimental

Master ingots of $Al_{75.5}Mn_{20.5}Si_4$ and $Al_{72.5}Mn_{17.4}Si_{10.1}$ were prepared by melting high-purity elements in an arc furnace. The icosahedral phase $Al_{75.5}Mn_{20.5}Si_4$ was prepared by melt spinning, and it is now realized that single-phased *i*-phase samples can only be prepared within a narrow range of AlMnSi contents [18]. Since this system is not thermodynamically stable, the structural order is not improved by annealing. The resistivity of these samples is typically $\rho(300\,\mathrm{K}) \approx 800\,\mu\Omega\,\mathrm{cm}$ ($\sigma(300\,\mathrm{K}) \approx 1250\,\Omega^{-1}\mathrm{cm}^{-1}$) and $\rho(4.2\,\mathrm{K})/\rho(300\,\mathrm{K}) \approx 1.15$ [19, 20]. The *i*-AlMnSi system is more disordered than other thermodynamically stable quasicrystals, having a relatively low correlation length ξ of several hundred Å [21], compared to that of $\approx 1\,\mu$m of the AlCu(Fe, Ru) system [22], implying that the *i*-AlMnSi system resembles an icosahedral glass [23].

Samples of $Al_{72.5}Mn_{17.4}Si_{10.1}$ for study of the approximant phase were cut from the master ingots and annealed. Although samples with x-ray diffraction patterns of an almost pure α-phase could be produced by annealing over a wide range of temperatures, small amounts of metallic impurity phases in high resistivity materials, even amounts which are not detectable by x-ray diffraction ($\leqslant 2\%$), can dramatically affect the measured electron transport properties. Therefore, the resistivity data is a convenient indicator of sample quality. As the annealing temperature was increased, both the resistivity values $\rho(300\,\mathrm{K})$ and the resistivity ratios $\rho(0.5\,\mathrm{K})/\rho(300\,\mathrm{K})$ increased. Samples of the highest quality were prepared by annealing between 600–680°C for two days. The resistivity of these samples is typically $\rho(300\,\mathrm{K}) \approx 3100\,\mu\Omega\mathrm{cm}$ ($\sigma(300\,\mathrm{K}) \approx 325\,\Omega^{-1}\mathrm{cm}^{-1}$) and $\rho(0.5\,\mathrm{K})/\rho(300\,\mathrm{K}) \approx 2$ [24]. Comparing these resistivities and resistivity ratios with the respective numbers of the *i*-phase (above) one sees that the approximant phase is even closer to the hypothetical 'perfect' quasicrystal than the *i*-phase. This is not too surprising, in view of the fact that the *i*-phase is merely a sort of metastable icosahedral glass, whereas the approximant is a well ordered and thermodynamically stable phase.

The icosahedral sample used in the optical measurements was a thin ribbon, $\approx 1 \times 1$ mm square and ≈ 20 microns thick. The surface of the ribbon was irregular and the material itself was very brittle, making it difficult to polish. An unpolished piece of ribbon was first supported by placing a thin coat of epoxy on one side; this side was then glued with epoxy to the apex of a pyramidal cone. The reflectance was measured by illuminating the entire

surface area of the ribbon; light that misses the sample was reflected out of the beam by the pyramid. To correct for the sample size and the irregular surface, the sample was coated over with gold (or aluminium) *in situ*, and the measurements repeated. The reflectance was then taken to be the ratio of the reflected intensity from the sample to that from the overcoated sample. We estimate the accuracy of the reflectance below $\approx 5000\,\mathrm{cm}^{-1}$ to be $\pm 1\%$ using this technique. However, a light spot which is smaller than the samples was used for higher-frequency measurements. Thus, the error of the reflectance could be larger at high frequencies. The experimental apparatus and the overcoating technique have been described in detail elsewhere [25].

The cut ingots from the approximant phase yielded a large surface area that was easily polished. However, this material exhibits porosity, and the overcoating technique was used in this case as well to correct for the irregular microstructure of the sample.

Reflectance measurements in the far-infrared region (50–700 cm^{-1}) were made at three different temperatures (295 K, 80 K and 10 K for the icosahedral phase, and 295 K, 180 K and 80 K for the approximant phase). In the infrared, visible and ultraviolet (700–46 000 cm^{-1}) regions, the reflectance was measured at room temperature only. The optical constants were calculated by a Kramers–Kronig analysis [26] of the power reflectance and at high frequency by ellipsometry.

The Kramers–Kronig transformations were done by extending the reflectance as follows: below the lowest measured frequency ($\approx 50\,\mathrm{cm}^{-1}$) the reflectance was matched and extrapolated to zero frequency by assuming the sample to be metallic and using the Hagen–Rubens form, $1 - R \propto \sqrt{\omega}$.

The high-frequency data in both the icosahedral and approximant phases is complicated by the presence of a strong interband transition. While the reflectance is seen to increase in both materials at $\approx 25\,000\,\mathrm{cm}^{-1}$, it is observed to turn flat at $\approx 42\,000\,\mathrm{cm}^{-1}$. The high-frequency extrapolation to the reflectance was constructed from a set of Lorentzian oscillators:

$$\tilde{\epsilon}(\omega) = \epsilon_\infty + \sum_i \frac{\omega_{pi}^2}{\omega_i^2 - \omega^2 - i\gamma_i\omega} \tag{1}$$

where ω_{pi} is the plasma frequency, ω_i the frequency of the oscillator, and γ_i the damping of the ith oscillator; ϵ_∞ is a term for the background dielectric constant. The number, position and strength of the oscillators was chosen to roughly agree with the flat region of the reflectance in the 20 000–30 000 cm^{-1} region, and to merge smoothly with the experimental data above 40 000 cm^{-1}; the reflectance has been extended using this oscillator model to $5 \times 10^5\,\mathrm{cm}^{-1}$. It is worth noting that this extrapolation gives results that are similar to the ω^{-2} extension, which is often used to simulate the reflectance in the region of interband transitions. Above $5 \times 10^5\,\mathrm{cm}^{-1}$, the reflectance was extended as ω^{-4} to simulate the behaviour of free electrons. The room-temperature data has been scaled to match the low-temperature measurements in the far infrared.

The results of the Kramers–Kronig analysis are sensitive mainly to the range of the interband transitions; this region has been extended to $5 \times 10^5\,\mathrm{cm}^{-1}$ in these calculations because at this point the extrapolation agrees with the measured reflectance of a number of transition metals [27] and transition-metal alloys [28]. The conductivity sum rule has been calculated to give the effective electron number density. The atomic number density can be derived from the mass density. Dividing the electron number density by the atomic number density, we obtain the mean valences (the average valence electrons per atom). Different high-frequency extrapolations (different widths for the interband region) have been tested,

corresponding to the mean valences $Z = 1.5$, 1.75 and 2.0. Below ≈ 1 eV the results are generally insensitive to the nature of the high-frequency extrapolations. However, above 1 eV the results are not as reliable. The high-frequency extrapolation we used gives the mean valence $Z \approx 1.75$, which is consistent with the value suggested by the study of stability of face-centred icosahedral (FCI) quasicrystals [29]. The Kramers–Kronig analysis yields the complex dielectric function

$$\tilde{\epsilon}(\omega) = \epsilon_1(\omega) + i\epsilon_2(\omega) = \epsilon_1(\omega) + \frac{4\pi i}{\omega}\sigma_1(\omega) \qquad (2)$$

where ϵ_1 is the real part of the dielectric function, and σ_1 is the frequency-dependent conductivity.

Ellipsometry is an accurate method used to determine the optical constants of materials [30], and the results do not depend on extensions to spectral regions where direct measurements are missing. It gives the real and the imaginary parts of the dielectric function without Kramers–Kronig analysis. However, the ellipsometric data normally are available within the limited region 1.4–6 eV. A method was used to correct the results of the Kramers–Kronig analysis of the reflectance with the ellipsometric data so that the effects due to the extrapolations could be eliminated [31]. The difference between the phase calculated from the Kramers–Kronig analysis of the reflectance and the phase from ellipsometric measurements is fitted by a polynomial of odd power. Then, the fitted polynomial was used to correct the phase of Kramers–Kronig analysis over all the frequency range. The other optical constants can be calculated from the corrected phase and the measured reflectance. The accuracy of this method is determined by the accuracy of the ellipsometric measurements and that of the reflectance measurements. The ellipsometric measurements were performed on both the icosahedral and approximant samples to remove the effects of extrapolations. Below 1 eV, the optical conductivity results are essentially not affected by the phase correction. This is consistent with the results of the different extrapolation tests.

3. Results

3.1. i-$Al_{75.5}Mn_{20.5}Si_4$

The reflectance of *i*-$Al_{75.5}Mn_{20.5}Si_4$ is shown in figure 1 from 60–38 000 cm^{-1} at 295 K and from 60–700 cm^{-1} at 80 K (the 10 K data is indistinguishable from the 80 K data and has been omitted). The reflectance decreases quickly with increasing frequency reaching a value of ≈ 0.55 at 5000 cm^{-1}, above which it remains relatively constant until the onset of interband transitions at $\approx 25\,000$ cm^{-1}. The various data above 38 000 cm^{-1} are different extrapolations. The inset in figure 1 details the 60–700 cm^{-1} region. The only feature in this region is a broad shoulder in the reflectance at 200 cm^{-1}, and the spectra display little temperature dependence.

The optical conductivity of *i*-$Al_{75.5}Mn_{20.5}Si_4$ is shown in figure 2. The full curve denotes the conductivity from 60–38 000 cm^{-1} at 295 K calculated by the Kramers–Kronig analysis and then corrected with the ellipsometric results. The broken curve represents the more direct results in the region of 11 000–46 000 cm^{-1} at the same temperature the ellipsometric measurements. The conductivity starts out from a low DC value and rises linearly as the frequency increases until it reaches a maximum at $\approx 18\,000$ cm^{-1} above which it decreases slowly. The inset in figure 2 shows the linear behaviour of the conductivity in the frequency region below 8000 cm^{-1}. A straight line is fitted to the conductivity data in the 500–8000 cm^{-1} region. The zero-frequency intercept of 1355 $\Omega^{-1}cm^{-1}$ of the fitted line is in

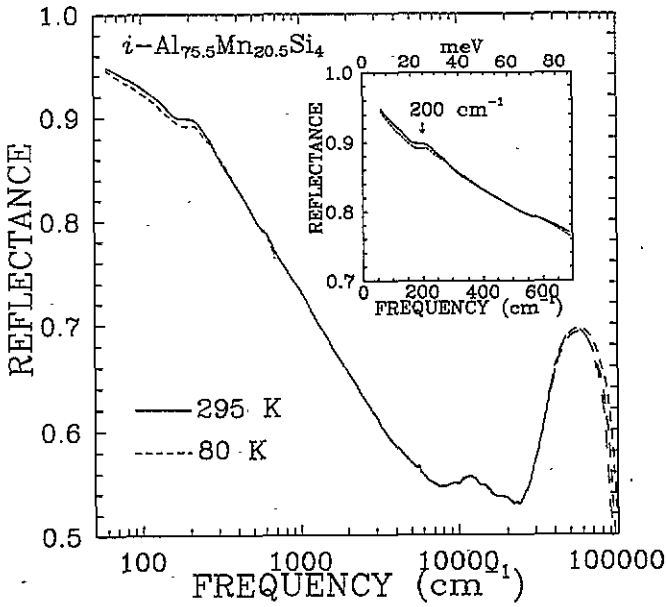

Figure 1. Reflectance of metastable icosahedral quasicrystal $Al_{75.5}Mn_{20.5}Si_4$ from $\approx$ 60–38 000 cm^{-1} at 295 K (full curve) and from $\approx$ 60–700 cm^{-1} at 80 K (broken curve); the 10 K data is indistinguishable from the 80 K data and has been omitted. The data sets above 38 000 cm^{-1} are from the extrapolations, and from bottom to top the longest-dash broken curve, the long-dash broken curve and the short-dash broken curve correspond to the mean valences $Z = 1.5$, 1.75 and 2.0, respectively. Inset: the reflectance in the 60–700 cm^{-1} region at 295 K and 80 K. The only feature in this region is a weak shoulder at 200 cm^{-1}.

good agreement with the DC-conductivity value of $\approx 1250\,\Omega^{-1}cm^{-1}$ [19, 20]. However, the low-frequency conductivity departs from its linear behaviour.

The optical conductivity in the low-frequency region from 60–700 cm^{-1} is shown in figure 3 at 295 K and 80 K. (The 10 K data is indistinguishable from the 80 K data and has been omitted). There is a prominent peak at 200 cm^{-1}, below which the conductivity appears to be increasing. In order to remove the 200 cm^{-1} feature, the spectra have been fitted to a single Lorentzian oscillator plus a linear background. The results of the fit are listed in table 1. The inset in figure 3 shows the optical conductivity with the feature removed. Below 400 cm^{-1}, the conductivity is clearly increasing as the frequency is lowered and deviates from the linear behaviour seen at higher frequencies. By extrapolating the data below 150 cm^{-1} to zero frequency, we obtain the values of zero-frequency conductivities of $\approx 1800\,\Omega^{-1}\,cm^{-1}$ at 295 K and $\approx 1600\,\Omega^{-1}\,cm^{-1}$ at 80 K, which are substantially higher than the DC values. However, the change of about 11% between the two temperatures is in rough agreement with transport measurements.

3.2. α-$Al_{72.5}Mn_{17.4}Si_{10.1}$

The reflectance of the 1/1 crystalline approximant α-$Al_{72.5}Mn_{17.4}Si_{10.1}$ of the icosahedral system is shown in figure 4 from 50–46 000 cm^{-1} at 295 K, and from 50–700 cm^{-1} at 180 K and 80 K. The reflectance at low frequency is $\approx$ 10% lower than in the icosahedral system, and decreases slowly reaching a value of ≈ 0.6 at 5000 cm^{-1}, above which it is essentially constant until the onset of interband transitions at $\approx$ 25 000 cm^{-1}, at which point the reflectance begins to increase. The data sets above 46 000 cm^{-1} are from the extrapolations.

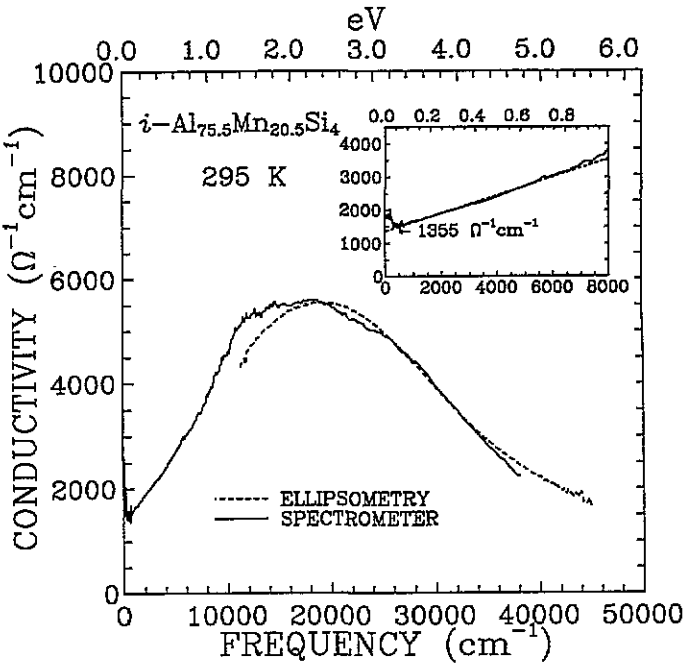

Figure 2. The optical conductivity of the metastable icosahedral quasicrystal $Al_{75.5}Mn_{20.5}Si_4$. The full curve denotes the data from 60 cm^{-1} to 38 000 cm^{-1} at 295 K which is calculated by the Kramers–Kronig analysis and then corrected with the ellipsometric results. The broken curve represents the results in the region of 11 000–46 000 cm^{-1} at the same temperature which is from the ellipsometric measurements. Inset: the low-frequency behaviour of the conductivity. The broken curve is a linear least-square fit to the data in the 500–8000 cm^{-1} region with an intercept.

The inset in figure 4 shows the 50–700 cm^{-1} range at several temperatures. In this region the nature of the reflectance differs sharply with that of the icosahedral phase; the broad feature at 200 cm^{-1} may now be resolved into *at least* nine phonon features and the temperature dependence is much larger (the arrows indicate the fitted oscillator frequencies).

The optical conductivity of α-$Al_{72.5}Mn_{17.4}Si_{10.1}$ is shown in figure 5. The full curve denotes the conductivity from 50 cm^{-1} to 40 000 cm^{-1} at 295 K which is calculated by the Kramers–Kronig analysis and then corrected with the ellipsometric results. The broken curve represents the conductivity in the region of 11 000–46 000 cm^{-1} obtained directly from ellipsometric measurements. The conductivity starts out from a low DC value (less than half the value of the icosahedral phase) and increases linearly until it reaches a maximum of $\approx 6000\ \Omega^{-1}$ cm^{-1} at $\approx 15\,000$ cm^{-1}, a typical value for most transition metals, above which it decreases slowly. It is interesting to note that despite having a lower conductivity at low frequencies, the conductivity in the near infrared is larger than that of the icosahedral phase. The inset in figure 5 shows the linear behaviour of the conductivity below 8000 cm^{-1} in more detail. The conductivity data in the 500–8000 cm^{-1} region has been fitted by using a straight line. The zero-frequency intercept of 374 Ω^{-1} cm^{-1} of the fitted line is in good agreement with the DC conductivity value of 325 Ω^{-1} cm^{-1} determined by transport measurements [24].

The optical conductivity in the 50–700 cm^{-1} range is shown in figure 6 at 295 K, 180 K and 80 K. The features seen in the reflectance may now be distinguished as a set of sharp phonon lines. The conductivity has been fitted by using classical oscillators (1) and a polynomial background to second order; the parameters are listed in table 1. The inset in

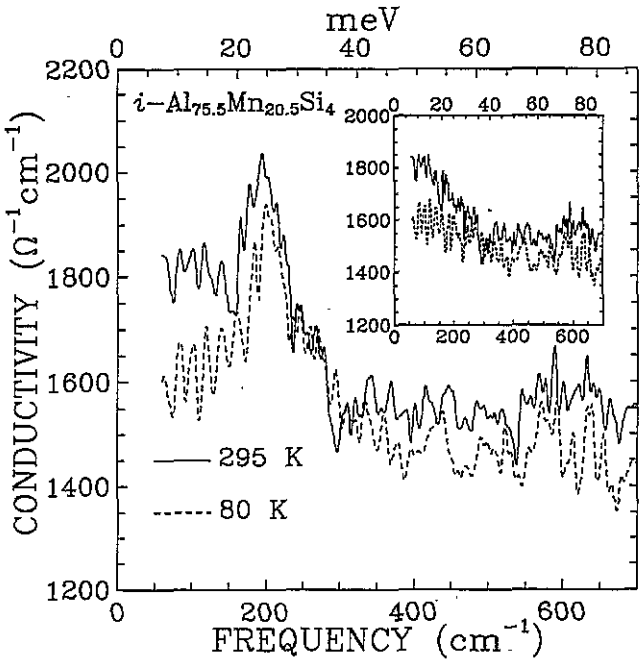

Figure 3. The optical conductivity of i-$Al_{75.5}Mn_{20.5}Si_4$ from $\approx 60\,cm^{-1}$ to $700\,cm^{-1}$ at 295 K (full curve) and 80 K (broken curve); the 10 K data is indistinguishable from the 80 K data and has not been shown. The only feature in this region is a peak at $200\,cm^{-1}$. Inset: the optical conductivity with the $200\,cm^{-1}$ feature removed reveals a conductivity which rises clearly below $\approx 400\,cm^{-1}$ and displays little temperature dependence.

Table 1. Parameters used to fit Lorentzian oscillators to the phonon peaks in the optical conductivity of i-$Al_{75.5}Mn_{20.5}Si_4$ and α-$Al_{72.5}Mn_{17.4}Si_{10.1}$. All frequencies are in cm^{-1}.

ω_i	γ_i	ω_{pi}	ω_i	γ_i	ω_{pi}	ω_i	γ_i	ω_{pi}
				i-$Al_{75.5}Mn_{20.5}Si_4$				
	295 K						80 K	
199	55	1067				206	75	1222
				α-$Al_{72.5}Mn_{17.4}Si_{10.1}$				
	295 K			180 K			80 K	
127	30	235	128	30	275	127	18	222
152	12	344	153	11	352	153	13	389
200	22	688	200	22	736	200	24	794
224	7	159	227	11	188	227	6	136
249	33	481	250	21	400	252	36	577
276	18	476	278	19	499	280	17	455
322	45	516	324	35	450	327	45	596
372	13	113	367	19	167	369	25	228
431	40	300	433	38	300	436	60	445

figure 6 shows the conductivity with the phonons removed and reveals a background, slowly decreasing with frequency. By extrapolating the lowest-frequency data of the conductivities to zero frequency, we obtain the zero-frequency estimates of $\approx 470\,\Omega^{-1}\,cm^{-1}$ at 295 K,

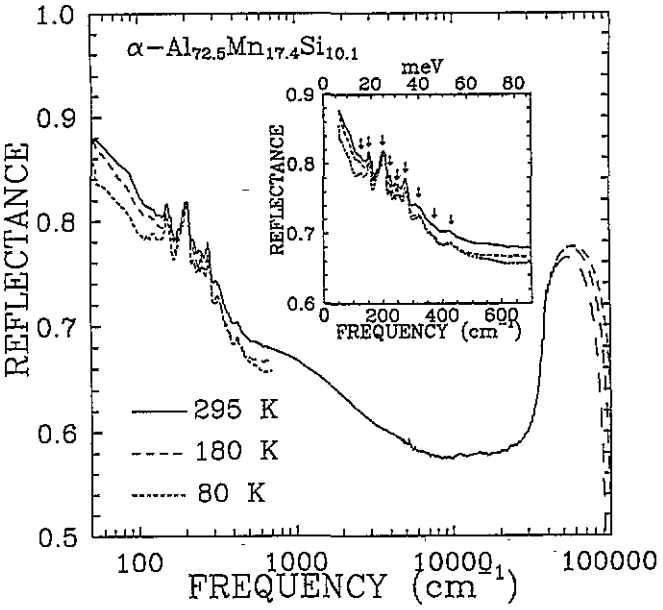

Figure 4. The reflectance of the α-$Al_{72.5}Mn_{17.4}Si_{10.1}$, the 1/1 crystalline approximant of *i*-$Al_{75.5}Mn_{20.5}Si_4$, from 50–46 000 cm^{-1} at 295 K (full curve) and from 50 cm^{-1} to 700 cm^{-1} at 180 K (long-dash broken curve) and 80 K (short-dash broken curve). The data sets above 46 000 cm^{-1} are from the extrapolations, and from bottom to top the longest-broken curve, the long-broken curve and the short broken curve correspond to the mean valences $Z = 1.5$, 1.75 and 2.0, respectively. Inset: reflectance in the 50–700 cm^{-1} region at several different temperatures. There are at least nine phonon lines that may be resolved (indicated from the arrows which represent the fitted oscillator frequencies).

$\approx 400\,\Omega^{-1}\,cm^{-1}$ at 180 K and $\approx 300\,\Omega^{-1}\,cm^{-1}$ at 80 K. The room-temperature value of the extrapolated zero-frequency conductivity is larger than that determined by fitting the linear region of the conductivity due to the deviation from linear behaviour at low frequencies.

4. Discussion

4.1. Electronic structure

The most remarkable feature of the optical conductivity in the icosahedral (figure 2) and approximant (figure 5) phases of AlMnSi is the total absence of a Drude response due to free electrons:

$$\sigma_D(\omega) = \frac{\omega_p^2 \Gamma}{4\pi(\omega^2 + \Gamma^2)} \tag{3}$$

where ω_p is the plasma frequency, Γ is the damping ($\Gamma = \hbar/\tau$), and ω is the frequency. The second feature is the peculiar linear behaviour of the conductivity below 1 eV (which has also been seen in perfect icosahedral quasicrystals [12]). These properties are unlike those of many metallic glasses that can be described by a Drude model in the strong-scattering limit [32]. The structure of the optical conductivity in both the approximant phase *and* the disordered icosahedral phase indicates that the free electrons' Drude contribution is swamped by other effects.

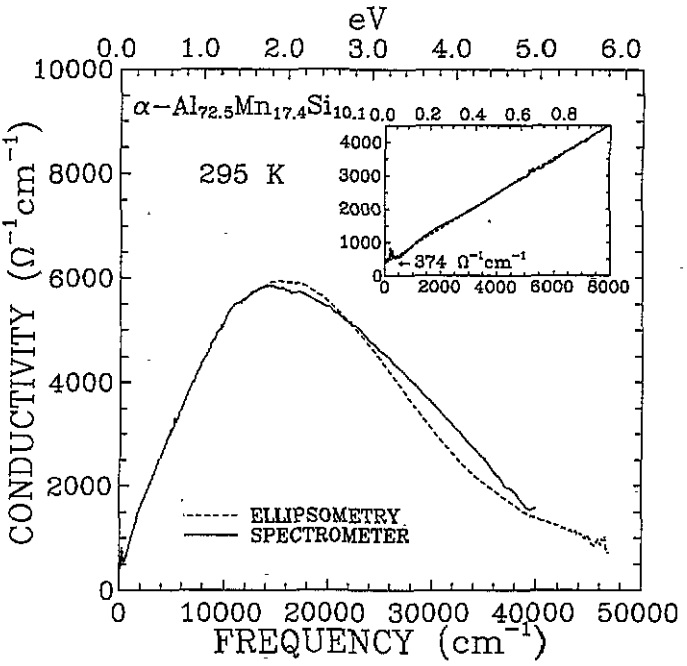

Figure 5. The optical conductivity of the 1/1 crystalline approximant α-$Al_{72.5}Mn_{17.4}Si_{10.1}$. The full curve denotes the data from 50 cm^{-1} to 40 000 cm^{-1} at 295 K which is calculated by the Kramers–Kronig analysis and then corrected with the ellipsometric results. The broken curve represents the results in the region of 11 000–46 000 cm^{-1} at the same temperature which is obtained by the ellipsometric measurements. Inset: the low-frequency behaviour of the conductivity. The broken curve is a linear least-squares fit to the conductivity in the 500–8000 cm^{-1} region with an intercept 374 Ω^{-1} cm^{-1}.

In good metals, such as aluminium, the room-temperature DC conductivity is $\sigma_0 \approx 5 \times 10^5\,\Omega^{-1}\,cm^{-1}$ ($\sigma_0 = n_e e^2\tau/m$ where n_e is the electron concentration, and τ is the scattering time at the Fermi surface, $n_e = 1.8 \times 10^{23}\,e\,cm^{-3}$ and $\tau = 0.5 \times 10^{-14}$ s for aluminium). However, the DC conductivity of the disordered icosahedral phase ($\approx 10^3\,\Omega^{-1}\,cm^{-1}$) is similar to that of a metallic glass of similar composition [33], and the value for the approximant phase is even lower ($\approx 325\,\Omega^{-1}\,cm^{-1}$) and close to those of the structurally ordered quasicrystals AlCuRu and AlCuFe. Moreover, the unusual Hall coefficient and thermoelectric power have been observed in the approximant phase [24], which is similar to that seen in the perfect AlCuRu and AlCuFe [10, 34]. Specific heat measurements on the approximant phase have shown that the density of states at the Fermi surface is lower than the free electron value [24]. In particular, Hall coefficient indicates that the number of carriers is very small ($\approx 10^{-2}\,e\,atom^{-1}$) [24].

The low conductivities observed in the structurally-ordered phases suggests the possibility of electronic localization. Electrons can behave as extended Bloch wave packets in crystals and exponentially localized waves in random systems. In one-dimensional quasicrystals, the calculations of electronic structure have shown that the energy spectrum is singular continuous (a Cantor set), i.e. neither continuous nor point-like, and the electronic wavefunctions are critical, i.e. neither extended nor localized [35, 36]. Based on model calculations, suggestions have been made that two- and three-dimensional quasicrystals also have singular continuous spectra and critical wavefunctions [37]. The little theoretical work that has been done on the electronic transport properties of quasicrystals can be used to

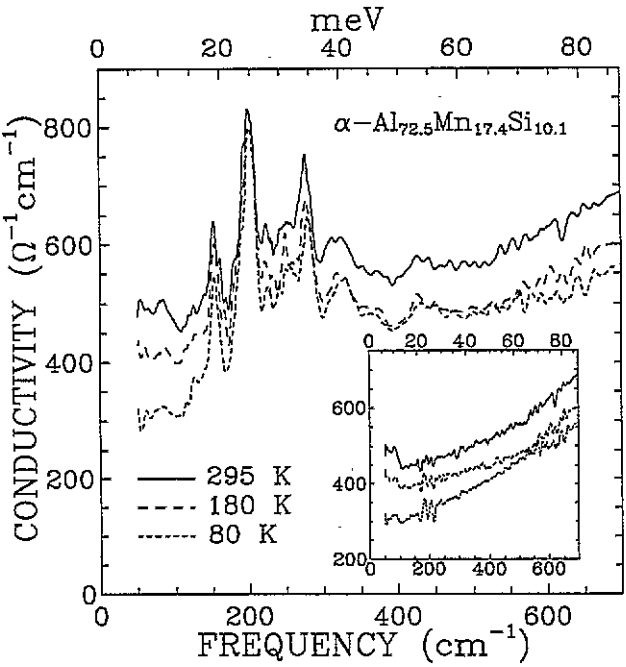

Figure 6. The optical conductivity of α-$Al_{72.5}Mn_{17.4}Si_{10.1}$ in the 50–700 cm^{-1} range at 295 K (full curve), 180 K (long-dash broken curve) and 80 K (short-dash broken curve). At least nine phonon features may be resolved. Inset: the optical conductivity with the phonons removed reveals a background with a quadratic nature.

advance arguments for either criticality [38] or localization [39]. However, the experimental investigations indicate that the electronic properties of quasicrystals may be due to band structure effects giving rise to a small number of carriers and a low density of states with extended electron wavefunctions [9].

The approximant phase is clearly a periodic structure, and as a result localization arguments based on a quasiperiodic potential do not apply; yet its optical properties, unlike the normal metals and many metallic glasses, cannot be described by the Drude formula. This suggests that the unusual behaviour of the optical conductivity in α-$Al_{72.5}Mn_{17.4}Si_{10.1}$ may be due to band structure effects. There is additional evidence to support this point of view. Band structure calculations have been performed on α-AlMnSi and show a sharp drop in the DOS at the Fermi surface and the formation of a pseudogap [15]. The similarity of the approximant and icosahedral phases, from both a structural and electronic point of view, implies that the anomalous optical conductivity of icosahedral phase is not due to the quasiperiodicity but the band structure effects which imply extended electronic wavefunctions.

Initial structural studies [40] and the measurement of the transport properties [41] of icosahedral alloys suggested that by assigning negative valences to the transition metals (TM) the Al–TM, quasicrystalline phases can be stabilized via the Hume–Rothery mechanism where the interaction of the Fermi surface with the Bragg planes is responsible for the formation of energy gaps in the electronic bands, producing kinks in the DOS and lowering the total energy of the system. Meanwhile, the band structure calculations for the crystalline approximant phases have shown that there are pseudogaps in the DOS at the Fermi energy E_F and the relationship $2k_F \approx G$ is satisfied, where the k_F is the Fermi

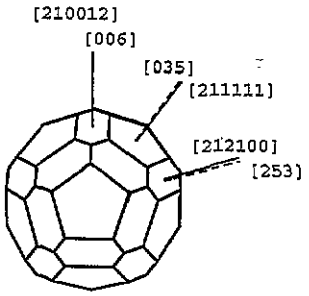

Figure 7. The Jones zone for the *i*-phase, constructed from the [211111] and [221001] planes and their equivalent, numbering 42 in all. The Jones zone of the approximant α-phase is visually indistinguishable from the icosahedral Jones zone. The full and the broken curves are typical reciprocal lattice vectors of the *i*-phase and the α-phase, respectively. The 12 fivefold directions of the *i*-phase are matched by 12 pseudo-fivefold vectors of the [530] family in the approximant, the angle between [211111] and [530] is only 0.76°. The 30 twofold directions of the *i*-phase ([210012] family) correspond to two families of the approximant: 24 vectors of the [253] family and 6 of [006] family. The former are 1.2° away from their icosahedral counterparts, the latter match exactly.

wavevector and the G a reciprocal lattice vector correspondent to a Bragg plane. Moreover, this mechanism could work more efficiently in the icosahedral quasicrystals than in the crystalline approximants because the icosahedral symmetry makes the Jones zone almost spherical.

In the case of a quasicrystal no Brillouin zone exists, because there is no shortest reciprocal lattice vector; rather, they fill the reciprocal space everywhere densely. Under these circumstances, the extended zone scheme should be preferred over the more familiar reduced scheme. In the extended zone scheme the quasimomentum k is not reduced to the Brillouin zone and, instead, varies over all of infinite reciprocal space. An analog of the Brillouin zone, however, exists: the Jones zone, constructed by planes perpendicular to the reciprocal lattice vectors associated only with prominent structure factors. The term 'prominent' is ambiguous unless a finite list of peaks qualifying for being 'prominent' is specified. (This ambiguity in selecting the 'prominent' peaks is responsible for the discrepancy between our and Carlsson's [42] Jones zones.) We base our choice on the measured diffraction pattern for *i*-$Al_{77}Mn_{20}Si_3$ (which is similar to the icosahedral phase examined here), which displays two prominent peaks for the [211111] and [221001] indices ([422222] and [442002] for the face-centred icosahedral quasicrystals) at $2.90\,\text{Å}^{-1}$ and $3.05\,\text{Å}^{-1}$ [43] (which are denoted as G_1 and G_2, respectively). The [211111] index along the fivefold axis has a multiplicity of 12 and the [221001] index along the twofold axis has a multiplicity of 30. Only these 42 peaks will be regarded as 'prominent', resulting in a nearly spherical Jones zone, shown in figure 7.

Electronic stabilization due to a Hume–Rothery mechanism implies that $2k_F \approx G$. In this case since $2k_F \approx 3\,\text{Å}^{-1}$, and $n_e = k_F^3/3\pi^2$, the electron densities in the icosahedral system must be $n_e \approx 1.14 \times 10^{23}\,\text{e cm}^{-3}$. If the atomic number density of the *i*-phase is similar to that of the α-phase, the average number of valence electrons per atom is $Z \approx 1.68$. This result is consistent with recent work which suggests that $Z \approx 1.75$ for all face-centred icosahedral quasicrystals [29]. A model based on the perturbation theory of a system of nearly-free electrons has been recently introduced [44] to explain the unusually low DC conductivities in icosahedral quasicrystals, as well as the linear behaviour of optical conductivity. The model asserts that given G_1, $G_2 \approx 2k_F$, then pseudogaps Δ_1 and Δ_2

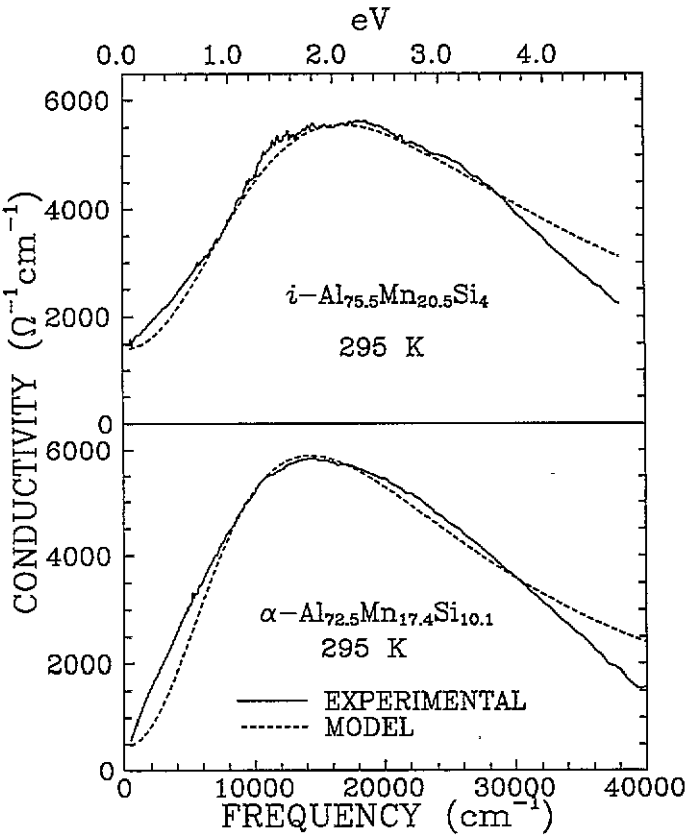

Figure 8. The result of the fit with the interband transition model of [44] to the room-temperature conductivity data of the i-$Al_{75.5}Mn_{20.5}Si_4$, top panel and α-$Al_{72.5}Mn_{17.4}Si_{10.1}$, bottom panel. The full curve is the measured optical conductivity and the broken curve is from the model with Drude and interband contribution of (4). The fitted gaps Δ and scattering rates $\hbar/\tau$ are 0.55 and 2.17 eV for the icosahedral and 0.5 and 1.8 eV for the approximant phases, respectively.

with parallel energy bands will appear at the Fermi surface due to splitting the degenerate states near the Bragg planes, destroying much of the Fermi surface and resulting in a low electron DOS. The contribution to the optical conductivity from a single Bragg plane has been previously expressed in an analytic form [45]. For an icosahedral alloy the total interband contribution will be the sum over all the pseudogaps Δ_1 (multiplicity 12) and Δ_2 (multiplicity 30). The values of these two pseudogaps are believed to be close to each other (and will be called Δ below).

For certain values of the parameters the general theoretical expression reduces to the following simple two-parameter formula [44]:

$$\sigma(\omega) = \frac{42}{6\pi^2}\frac{e^2 G}{\hbar}\frac{\pi}{2}\frac{\Delta}{\hbar}\tau\frac{(\omega\tau)^2}{[1+(\omega\tau)^2]^2}. \tag{4}$$

The results of fitting the model using a pseudogap Δ and a Drude contribution to i-$Al_{75.5}Mn_{20.5}Si_4$ at room temperature is shown in figure 8. A value of the pseudogap of $\Delta \approx 0.55$ eV is consistent with that found in ordered $Al_{63.5}Cu_{24.5}Fe_{12}$ [44]. The model produces an approximately linear behaviour at low frequencies, and the overall agreement with the experimental data is good.

The optical conductivity at low frequencies (the far-infrared region) in the icosahedral alloy clearly increases as the frequency is lowered, and at the lowest frequency it reaches a value which is much larger than the DC conductivity. As the temperature is lowered the conductivity appears to increase less rapidly with decreasing frequency. However, lower-frequency data is needed to see how the conductivity behaves as it approaches zero-frequency. It is not clear that this behaviour has been observed in other quasicrystals with larger coherence lengths [12].

The close resemblance of the two experimental conductivity curves of figure 8 can be easily explained in simple geometrical terms. Although the approximant phase, unlike the quasicrystal, possesses the shortest reciprocal vector and a Brillouin zone, the use of the extended zone scheme is still advisable. Indeed, the period of the lattice equals 12.8 Å resulting in a tiny Brillouin zone, approximately ten times smaller than the Jones zone of figure 7. The quasimomenta could be reduced to this tiny zone, and the band structure and even interband absorption could be numerically calculated. The band structure has indeed been calculated this way [15]. It shows an extremely complicated diagram with nearly 100 virtually flat bands, with the Fermi level located somewhere in the 50th or 70th band. This is the classical situation for which Jones proposed the use of the 'large' zones [46] (later called Jones zones after him). The same dispersion relations are made more comprehensible if the quasimomentum is not reduced to the Brillouin zone. Instead, a zone is built only of those Bragg planes which carry prominent Fourier components of the pseudopotential. Quite often the Fermi surface matches this zone quite well, which justifies the approach. In this case, the 50 or 70 bands below the Fermi level appear to be irrelevant for most physical properties and could be excluded from the consideration. Note that, if this approach is used, there remains little difference in the treatment of crystals and quasicrystals.

Accordingly, we build the Jones zones for the approximant phase by selecting the most prominent peaks in the experimental diffraction pattern. They are the [530], [532] and [600] peaks shown in figure 7 [47]. They have multiplicities of 12, 24, 6 with wavevectors of 2.89 $Å^{-1}$, 3.05 $Å^{-1}$ and 2.97 $Å^{-1}$, respectively [13]. The Jones-zone boundary consists of 12 pentagons of the [530] family and 30 hexagons (24 of [532] and 6 of [600]). The Jones zone appears to be so close to that of the icosahedral quasicrystal that the two are visually indistinguishable and, accordingly, we present one figure for both Jones zones (e.g. the angle between the true fivefold [211111] direction of the i-phase and pseudo-fivefold [530] of the approximant α-phase is about 1°.) Note that at this stage we exploit again Jones' approach: the short [100], [111] and similar reciprocal lattice vectors have been ignored, as well as the [350], while retaining the [530], even though the latter two are of the same length. This procedure is justified by the fact that, though the unit cell is cubic, the space group is tetragonal Pm3 [13] and, accordingly, [530] and [350] are not equivalent. (Pm3 allows cyclic permutations of all three indices, but not of two.) Thus, the symmetry does not require [350] to be of the same intensity as [530]. Moreover, the experimental diffraction patterns [13, 47] show that, while [530] is a dominating peak, [350] has no substantial intensity and must be neglected in the Jones construction. A similar procedure was applied to the [532] family and in discarding the [611] peak (accidentally degenerate with [532]). Note that in the Brillouin zone formalism all those peaks are equally treated, despite their unequal contributions, which makes the numerically calculated band structure virtually incomprehensible. A Jones-style approach similar to ours was adopted by Carlsson in his model band structure calculations [42].

After the close resemblance of the Jones zones of both the i- and α-phases has been revealed, the similarity in the $\sigma(\omega)$ curves is no longer surprising. One could arrive at the

same conclusion, the similarity between the two $\sigma(\omega)$ curves, in a more qualitative manner. Both the i- and α-phases are built from the same local icosahedral cluster, have similar compositions, lattice constants, etc. The optical conductivity in the eV range probes mainly these 'mid-range' properties, which are nearly identical in the two structures. The major difference between the atomic structures of i- and α-phases is in the way the clusters are assembled, i.e. in the long-range order at long wavelengths. Such a difference is more likely to exhibit itself in far infrared or even at lower energies. Indeed, we observe greater differences between the two $\sigma(\omega)$ curves in the infrared than in the visible part of the spectrum.

Accordingly, we treat the approximant α-phase with the plane-wave model [44] with three phenomenological pseudogaps for the three orbits. In the overdamped situation, as before, we could consider all three pseudogaps as being equal to each other, reducing the number of fitting parameters to two. The best fit is achieved with $\Delta \approx 0.5\,\mathrm{eV}$, which is similar to that in the icosahedral phase. Alternatively, the interband contribution could be in principal numerically calculated using eigenfunctions and eigenvalues in the Brillouin zone, but taking into account the necessity to sum contributions from something of the order of 50 flat bands would be numerically intensive.

4.2. Phonons

While the icosahedral and approximant phases display similar optical properties, the phonon features in these two systems are vastly different. In the approximant phase the phonons are clearly visible as a series of sharp lines in the 100–500 cm^{-1} range. The strongest lines have been fitted to classical oscillators (see table 1), which describe the system quite well. The total integrated oscillator strength (proportional to $\sum \omega_{pi}^2$) displays little or no temperature dependence. The results of the fit are sensitive to the choice of the background, and as a result the variations observed are most likely due to this uncertainty. In the absence of electron–phonon coupling, no change in the oscillator strength of the system with temperature is expected [48].

In the icosahedral phase, the sharp phonon lines observed in the approximant phase are no longer present; instead, they are replaced by a broad peak in the conductivity at 200 cm^{-1}. It is interesting to note that the location of this peak corresponds *exactly* to the most intense phonon peak in the approximant phase. There is some difficulty with noise at low temperatures, but it appears that the oscillator strength of this mode is increasing. A similar feature has been observed in the icosahedral quasicrystal $Al_{63.5}Cu_{24.5}Fe_{12}$ at 245 cm^{-1} [12], which is very close to the peak in the phonon DOS of aluminium. The proximity to the DOS peak in aluminium and an apparent temperature dependence of the oscillator strength implied that this feature was due to phonon excitations†. Initial studies of phonons in one-dimensional quasilattices predicted that low-frequency acoustic phonons would behave much as they would in periodic lattice, but that high-frequency phonons would have wavefunctions similar to the electron wavefunctions: neither localized nor extended, but critical [49]. In light of the results for the electronic properties of three-dimensional icosahedral systems, which imply that the electron wavefunctions are extended, it may similarly be argued that the phonon wavefunctions are also extended, as observed in inelastic neutron scattering measurements of phonons in i-AlCuLi [50]. The temperature dependence of the oscillator strength, if it truly exists, is difficult to interpret, and may

† The apparent decrease in the oscillator strength was initially thought to be due to the $n(\omega)+1$ Bose factor for a phonon at 245 cm^{-1}. However, it is not clear that the oscillator strength is changing substantially and furthermore, no change due to the Bose factor is expected [48].

indicate electron–phonon coupling. Alternatively, the structure could be interpreted as a transition between two discreet electronic states that straddle the Fermi level. However, this is unlikely, given that the peak in the icosahedral phase occurs in exactly the same position as the most intense phonon in the approximate phase.

5. Conclusions

The optical properties of the icosahedral quasicrystal $Al_{75.5}Mn_{20.5}Si_4$ and its low-order 1/1 crystalline approximant α-$Al_{72.5}Mn_{17.4}Si_{10.1}$ have been determined at several different temperatures. The optical conductivity indicates the presence of pseudogaps in both systems (which in general are quite similar) suggesting that the electronic properties of the icosahedral system are not a consequence of the quasiperiodic order of the system, and that a common mechanism is responsible for both systems. Band structure calculations that have been carried out for the approximant phase of α-$Al_{72.5}Mn_{17.4}Si_{10.1}$ [15] indicate the presence of a pseudogap in the DOS at the Fermi surface stabilized by Hume–Rothery conditions. The similarity of the optical properties of the icosahedral phase to the approximant phase on the optical properties implies that band structure arguments also apply to the icosahedral system and that the electron wavefunctions are extended, rather than localized. The studies on the structure and transport properties [40, 41] also show the evidence to suggest that the icosahedral phases are stabilized by Hume–Rothery arguments and that the interaction of Fermi surface with the Bragg planes results in the formation of pseudogaps and the reduction of electron DOS at Fermi surface. A model [44] based on two pseudogaps for parallel energy bands and a residual Drude component reproduces the data in the icosahedral and approximant phases quite well.

The phonons in the ordered approximant phase appear to collapse into a single broad feature in the disordered icosahedral phase; this feature is in exactly the same position as the most intense phonon in the approximant phase, ruling out the likelihood that this is an electronic transition. The presence of a phonon in the icosahedral system indicates that, as in the case of the electron wavefunctions, the phonon wavefunctions are probably extended for a three-dimensional icosahedral system.

Acknowledgments

We would like to thank C Kallin, N K Mukhopadhyay, N W Ashcroft and J Preston for valuable discussions. This work was supported by the Natural Science and Engineering Research Council (Canada) and the Canadian Institute for Advanced Research and the National Science Foundation Contract No DM90-15538.

References

[1] Shechtman D, Blech I, Gratias D and Cahn J W 1984 *Phys. Rev. Lett.* **53** 1951
[2] Wang N, Chen H and Kuo K H 1987 *Phys. Rev. Lett.* **59** 1010
[3] Bendersky L 1985 *Phys. Rev. Lett.* **55** 1461
[4] Ishimasa T, Nissen H-U and Fucano Y *Phys. Rev. Lett.* 1987 **55** 511
[5] Chen H, Li D X and Kuo K H 1988 *Phys. Rev. Lett.* **60** 1645
[6] DiVincenzo D P and Steinhardt P J (eds) 1991 *Quasicrystals: The State of the Art* (Singapore: World Scientific)
Steinhard P J and Ostlund S (eds) 1987 *The Physics of Quasicrystals* (Singapore: World Scientific)
[7] Tsai A P, Inoue A and Masumoto T 1987 *Japan. J. Appl. Phys.* **26** L1505
[8] Tsai A P, Inoue A and Masumoto T 1988 *Japan. J. Appl. Phys.* **27** L1587

[9] Poon S J 1993 *Adv. Phys.* **41** 303 1993
[10] Biggs B D, Poon S J and Munirathnam N R 1990 *Phys. Rev. Lett.* **65** 2700
[11] Klein T, Berger C, Mayou D and Cyrot-Lackman F 1991 *Phys. Rev. Lett.* **66** 2907
[12] Homes C C, Timusk T, Wu X, Altounian Z, Sahnoune A and Ström-Olsen J O 1991 *Phys. Rev. Lett.* **67** 2694
[13] Cooper M and Robinson K 1966 *Acta. Cryst.* **20** 614
[14] Elser V and Henley C L 1985 *Phys. Rev. Lett.* **55** 2883
Guyot P and Audier M 1985 *Phil. Mag.* B **52** L15
[15] Fujiwara T 1989 *Phys. Rev.* B **40** 942
Fujiwara T and Yokokawa Y 1990 *Quasicrystals (Springer Series in Solid State Sciences* **93**) ed. T Fujiwara and T Ogawa (Berlin: Springer)
[16] Fujiwara T and Yokokawa T 1991 *Phys. Rev. Lett.* **63** 333
[17] Hafner J and Krajci M 1992 *Phys. Rev. Lett.* **63** 333
[18] Yamane H, Kimura K, Shibuya T and Takeuchi S 1987 *Mat. Sci. Forum* **22–24** 539
[19] Kimura K, Hashimoto T and Takeuchi S 1986 *J. Phys. Soc. Japan* **55** 1810
Kimura K and Takeuchi S 1991 *Quasicrystals: The State of the Art* ed. D P DiVincenzo and P J Steinhardt (Singapore: World Scientific)
[20] Biggs B D, Pierce F S and Poon S J 1992 *Europhys. Lett.* **19** 415
[21] Bancel P A, Heiney P A, Stephens P W, Goldman A I and Horn P M 1985 *Phys. Rev. Lett.* **54** 2422
[22] Guryan C A, Goldman A I, Stephens P W, Hiraga K, Tsai A P, Inou A and Masumoto T 1989 *Phys. Rev. Lett.* **62** 2409
[23] Robertson J L and Moss S C 1991 *Phys. Rev. Lett.* **66** 353
Stephens P W and Goldman A I 1991 *Sci. Am.* **44** (April)
[24] Biggs B D, Pierce F S and Poon S J 1992 *Europhys. Lett.* **19** 415
[25] Homes C C, Reedyk M, Crandles D A and Timusk T 1993 *Appl. Opt.* **32** 2976
[26] Wooten F 1972 *Optical Properties of Solids* (New York: Academic)
[27] Palik E D (ed) 1991 *Handbook of Optical Constants of Solids II* (New York: Academic)
[28] Seib D H and Spicer W E 1970 *Phys. Rev.* B **2** 1676, 1694
[29] Tsai A P, Yokoyama Y, Innoue A and Matsumoto T 1992 *Physics and Chemistry of Finite Systems: From Clusters to Crystals (NATO ASI Series* **374**) ed. P Jena, S N Khanna and B K Rao (Dordrecht: Kluwers) p 177
[30] Aspnes D E 1985 *Handbook of Optical Constants of Solids* ed. E D Palik (New York: Academic)
[31] Bozovic I 1990 *Phys. Rev.* B **42** 1969
[32] McKnight S W and Ibrahim A K 1984 *J. Non-Cryst. Solids* **61/62** 1301
[33] Kimura K, Yamane H, Hashimoto T and Takeuchi S 1987 *Mat. Sci. Forum* **22–24** 471
[34] Biggs B D, Li Y and Poon S J 1991 *Phys. Rev.* B **43** 8747
[35] Kohmoto M, Sutherland B and Tang C 1987 *Phys. Rev.* B **35** 1025
[36] Bellissard J, Iochum B, Scoppola E and Testard D 1989 *Commun. Math. Phys.* **125** 527
[37] Fujiwara T and Tsunetsugu H 1991 *Quasicrystals: The State of the Art* ed. D P DiVincenzo and P J Steinhard (Singapore: World Scientific)
[38] Tsunetsugu H and Ueda K 1991 *Phys. Rev.* B **43** 8893
[39] Kitaev A Yu 1988 *Sov. Phys.–JETP Lett.* **487** 299
Kitaev A Yu 1990 *Proc. Adriatico Research Conf. on Quasicrystals* ed. M V Jaric and S Lundqvist (Singapore: World Scientific)
[40] Bancel P A and Heiney P A 1986 *Phys. Rev.* B **33** 7917
[41] Wagner J L, Wong K M and Poon S J 1989 *Phys. Rev.* B **39** 8091
[42] Carlsson A E 1993 *Phys. Rev.* B **47** 2515
[43] Nanao S, Tanaka Y, Sakurai Y, Kokubu C, Watanabe Y, Matsuda M and Yasui I 1988 *Mat. Sci. Eng.* **99** 427
[44] Burkov S E, Timusk T and Ashcroft N W 1992 *J. Phys.: Condens. Matter* **4** 9447
[45] Ashcroft N W and Strum K 1971 *Phys. Rev.* **3** 1898
[46] Mott N F and Jones H 1975 *The Theory of the Properties of Metals and Alloys* (Oxford: Clarendon)
Jones H 1975 *The Theory of Brillouin Zones and Electronic States in Crystals* (Amsterdam: North-Holland)
[47] Koskenmaki D C, Chen H S and Rao K V 1986 *Phys. Rev.* B **33** 5328
[48] Burstein E 1964 *Phonons and Phonon Interactions* ed. Bak T A (New York: Benjamin)
[49] Machida K and Fujita M 1986 *J. Phys. Soc. Japan* **55** 1799
[50] Goldman A I, Stassis C, Bellisent R, Moudden H, Pyka N and Gayle F W 1991 *Phys. Rev.* B **43** 8763